

Superconducting current and low-energy states in a mesa-heterostructure interlayered with a strontium iridate film with strong spin-orbit interaction

A. M. Petrzlik,¹ K. Y. Constantinian,¹ G. A. Ovsyannikov,¹ A. V. Zaitsev,¹ A. V. Shadrin,^{1,2} A. S. Grishin,¹ Yu. V. Kisilinski,¹ G. Cristiani,³ and G. Logvenov³

¹*Kotel'nikov IRE RAS, Mokhovaya 11-7, Moscow, 125009, Russia*

²*Moscow Institute of Physics and Technology, Dolgoprudny, Moscow Region, 141701, Russia*

³*Max Planck Institute for Solid State Research, Stuttgart, 70569, Germany*



(Received 6 February 2019; revised manuscript received 17 June 2019; published 8 July 2019)

The superconducting current has been observed in mesa-heterostructures Nb/Sr₂IrO₄/YBa₂Cu₃O_x with a Sr₂IrO₄ interlayer having strong spin-orbit interaction. The superconducting critical current density $j_c \approx 0.3$ A/cm² for $d = 7$ nm was registered at $T = 4.2$ K. Magnetic-field dependence of superconducting critical current $I_c(H)$ showed a sharp central peak and minor oscillating behavior for sidelobes indicated the absence of pinholes. Integer and fractional Shapiro steps were observed at voltages $V_{m,n} = (m/n)(h/2e)f_e$ under microwave radiation at frequencies $f_e = 38$ GHz and $f_e = 50$ GHz. Fractional Shapiro steps ($m/n = 1/2, 3/2$) point on the presence of the second harmonic in the superconducting current-phase relation. The zero-bias conductance peak was observed hinting on existence of low-energy states at Sr₂IrO₄/YBa₂Cu₃O_x interface at temperatures higher than the superconducting critical temperature of Nb.

DOI: [10.1103/PhysRevB.100.024501](https://doi.org/10.1103/PhysRevB.100.024501)

I. INTRODUCTION

In recent years development of Josephson junctions featuring spin-dependent processes attracts increasing interest [1,2]. Recently it was shown theoretically that spin-orbit interaction (SOI) leads to generation of spin-triplet superconducting current [1–6]. Particularly, it was predicted that the SOI in the ferromagnet F of a superconductor-ferromagnet-superconductor (S - F - S) junction results in a pure spin-triplet state without any singlet superconductivity, and this state persists throughout the ferromagnetic interlayer [4–7]. In Ref. [8] magnetoelectric effect and spin-triplet pairing were predicted for the case when ferromagnetic interlayer F was replaced by the normal-metal N with SOI, and superconducting current was analyzed. The S/N interface for the case of strong SOI in N was analyzed in Ref. [9], and it has been shown that the robust spin-triplet pairing due to proximity effect takes place, and promotes the interference of superconducting wave function of superconductors (Josephson effect). However, most of experimental investigations of impact of SOI on Josephson effect were performed in structures with superconductors linked by topological insulator (semiconductor) underlayer. The unconventional proximity effect was observed in Nb superconducting junction with a magnetically doped topological insulator (Fe-Bi₂Te₂Se), and the splitting of zero-bias conductance peak and the conductance oscillations affected by microwaves have been reported [10]. One possibility to replace the topological insulator with a semiconductor film with SOI was suggested in Ref. [11], stimulating extensive theoretical and experimental studies. Superconductor-semiconductor-superconductor Al/InAs/Al junction was experimental studied in Ref. [12] and the asymmetry of interference pattern was discussed under suggestion of impact of strong SOI. The appearance of the 4π -periodic superconducting current-phase

relation (CPR) was analyzed for a junction with semiconductor superconducting wire [13]. An unconventional CPR in topological Josephson junctions was reported and analyzed in Refs. [14,15], and for the case of a wire with SOI, in which fractional $1/2$ electron charge may form along with 8π -periodic CPR [16].

A promising choice of material with strong SOI for superconducting junction is the $5d$ transition-metal oxide Sr₂IrO₄ [17–20]. This compound is known as a canted antiferromagnetic insulator with the band splitting [21,22]. The intrinsic crystal field ~ 0.4 eV [21] splits the degenerate states of $5d$ electrons into e_g and t_{2g} bands, and the partially filled t_{2g} band splits into $J_{\text{eff}} = 3/2$ and $J_{\text{eff}} = 1/2$ due to the strong SOI over the iridium ions. Unconventional properties of Sr₂IrO₄, and the interfaces with other oxides, particularly with the superconducting cuprate are discussed in Refs. [23–25]. Moreover, Sr₂IrO₄ [26–28] gives opportunities for spin manipulation in a junction with the barrier material with weak magnetic moment.

For experimental studies a sandwich-type structure seems preferable due to the possibility to reduce the distance between superconductors down to a few nanometers thick that is necessary for the interference of superconducting wave functions in the junction. An inclusion of high- Z metallic Pt into the ferromagnetic interlayer for experimental study of impact of SOI on superconducting proximity effect was reported [29].

In this paper we present experimental results on observation of superconducting current and study of electron and microwave transport characteristics of hybrid superconducting Nb/Au/Sr₂IrO₄/YBa₂Cu₃O_x sandwich-type mesa-structures with nanometer thickness of the Sr₂IrO₄ interlayer.

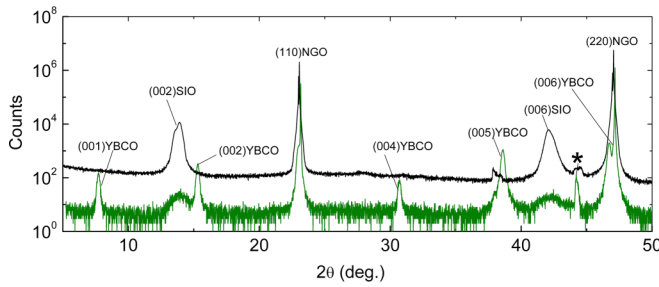


FIG. 1. X-ray-diffraction patterns of Bragg reflections for 17-nm-thick Sr_2IrO_4 (marked SIO, the upper curve), and for heterostructure $\text{Au}/\text{Sr}_2\text{IrO}_4/\text{YBa}_2\text{Cu}_3\text{O}_x$ (lower curve) grown on NdGaO_3 (marked NGO). The thicknesses of Au, Sr_2IrO_4 , and $\text{YBa}_2\text{Cu}_3\text{O}_x$ (marked YBCO) films were 10, 7, and 60 nm, correspondingly. Symbol “**” points on response from sample holder.

II. EXPERIMENTAL SAMPLES

The thin bilayers of $\text{YBa}_2\text{Cu}_3\text{O}_x$ (YBCO) and Sr_2IrO_4 with thickness 60–70 nm and 5–7 nm, correspondingly, were grown epitaxially by pulsed-laser deposition (PLD) on (110) NdGaO_3 (NGO) single-crystalline substrates. A KrF-excimer laser with frequency 10 Hz and 1.6-J/cm² energy density was used to ablate materials from YBCO and Sr_2IrO_4 stoichiometric targets. The bottom YBCO thin film was deposited at 830 °C in an oxygen atmosphere of 0.5 mbar. The Sr_2IrO_4 thin film was deposited at 700 °C in an argon atmosphere with pressure 0.5 mbar. Both YBCO and Sr_2IrO_4 films were grown with the c axis perpendicular to the substrate plane [25]. Note, high-quality epitaxial Sr_2IrO_4 thin films with thickness up to 300 nm have been grown by PLD on SrTiO_3 (001) substrates [30]. A protective Au thin film with thickness about 10 nm was deposited *in situ* at 30 °C in the PLD chamber. The superconducting Nb film with thickness about 200 nm was deposited *ex situ* by magnetron sputtering in an argon atmosphere at room temperature, followed after sputtering of Au film [31]. The crystalline parameters of the Sr_2IrO_4 film and the bilayer $\text{Sr}_2\text{IrO}_4/\text{YBCO}$ were determined using the four-circle x-ray diffractometer, measuring $2\Theta/\omega$ scans and rocking curves. The x-ray diffraction (XRD) patterns of Bragg reflections of the reference Sr_2IrO_4 film and for heterostructure $\text{Au}/\text{Sr}_2\text{IrO}_4/\text{YBCO}$ are given in Fig. 1. XRD data show that the lattice parameter $c = 1.283$ nm was obtained for Sr_2IrO_4 with thickness $d = 17$ nm and $c = 11.66$ nm for $\text{YBa}_2\text{Cu}_3\text{O}_x$ film.

$\text{Nb}/\text{Au}/\text{Sr}_2\text{IrO}_4/\text{YBCO}$ mesa-structures (MS) with square shape and sizes from $A = L^2 = 10 \times 10 \mu\text{m}^2$ to $50 \times 50 \mu\text{m}^2$ (total five MS on a chip) were formed using optical lithography, reactive ion-plasma etching, and ion-beam etching at low ion accelerating voltages. Oxygen plasma treatments were performed after each lithography process to remove remains of the resist. The SiO_2 protective insulator layer was deposited by rf sputtering provided the DC current to flow in perpendicular direction to the MS layers. An additional Nb (or NbN) film with a thickness of 200 nm was sputtered providing superconducting current transport through the DC wiring. Contact pads were made of gold films for four-point I - V curve measurements (see Fig. 2).

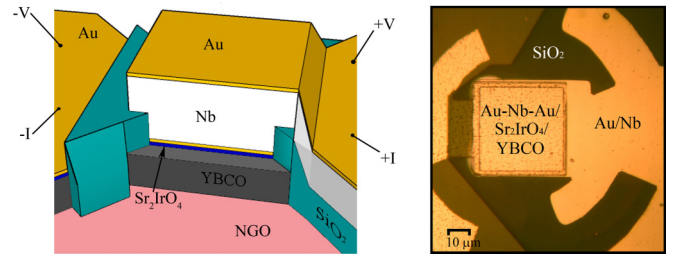


FIG. 2. Sketch of 3D view (on the left) and the top photo (on the right) of the mesa-heterostructure $\text{Nb}/\text{Au}/\text{Sr}_2\text{IrO}_4/\text{YBCO}$. The insulating SiO_2 layer separates top and bottom electrodes and provides electrical transport along the c axis. Four-probe current supply and voltage measurement wires are shown schematically.

III. RESULTS AND DISCUSSION

A. DC transport characteristics

The normal resistance of the Nb/Au interface was in the $\mu\Omega$ range and $R_{\text{Nb}/\text{Au}}A \sim 10^{-5} \mu\Omega \text{cm}^2$, which corresponds to the Nb/Au interface transparency $\mathfrak{T}_{\text{Nb}/\text{Au}} \approx 1$ [31,32]. The averaged value of the normal resistance for four MS on one chip with Sr_2IrO_4 thickness $d = 7$ nm was $R_NA \approx 100 \mu\Omega \text{cm}^2$ at $T = 4.2$ K (see Table I). The contribution of resistivity from Sr_2IrO_4 film $\rho \times d = 7 \times 10^3 \mu\Omega \text{cm}^2$ ($d = 7$ nm) should be much higher (see Supplemental Material [32]). A tunneling through a high-resistive barrier can explain the measured value of R_NA and allows one to argue that the transport through the $\text{YBCO}/\text{Sr}_2\text{IrO}_4$ and $\text{Sr}_2\text{IrO}_4/\text{Au}$ interfaces in the MS with a total transparency $\mathfrak{T} = 3 \times 10^{-5}$ is the main mechanism for electrical transport [31]. Three MS for $d = 7$ nm and $L = 50, 40,$ and $30 \mu\text{m}$ show relatively good reproducibility of the $I_C R_N$ product. The smaller one, $L = 20 \mu\text{m}$, had 3 times smaller critical current density $j_C = I_C/A$, but R_NA differs not too much (Table I). The fifth MS on the same chip with $L = 10 \mu\text{m}$ had much higher R_NA and was omitted. Parameters of two MS with $d = 5$ nm are also given in Table I.

The critical current I_C was evaluated from the I - V curve using also the plot of differential resistance $R_D = dV/dI$ [see Fig. 3(a)]. At temperatures near T_{CNb} (critical temperature of Nb film) the amplitudes of I_C were small and its values were determined from $R_D(I)$ since the influence of fluctuations resulted in “rounded” I - V curves. In this case an approach described in Ref. [33] (see also Supplemental Material [32]) was used which takes into account the external low-frequency fluctuations [33,34]. Temperature dependences of $I_C(T)$ and the voltage of singularity on $R_D(V)$ caused by the energy gap of the Nb electrode $V_\Delta(T)$ are given in Fig. 3(b) and BCS dependence of Nb gap with $T_{\text{CNb}} = 8.4$ K is also presented. The singularity on conductivity $G(V)$ caused by the energy gap of the Nb electrode is clearly seen at $T = 4.2$ K at $V = V_\Delta$ as shown in the inset to Fig. 3(b). The singularities of $R_D(V)$ corresponding to superconducting current at $V = 0$ are also shown for temperatures $T = 4.2$ K and $T \simeq T_{\text{CNb}} = 8.4$ K. Obtained dependence of $I_C(T)$ is proportional to the Nb gap as it follows for the junction of two superconductors with different superconducting gaps [35]. Reducing the thickness of Sr_2IrO_4 interlayer from 7 to 5 nm the R_NA decreases,

TABLE I. DC parameters of the mesa-structures fabricated on the same substrate, $T = 4.2$ K. L is the planar size of the MS, square $A = L^2$, I_C is critical current, R_N is normal resistance measured at $V = 0.8$ mV, $j_C = I_C/A$ is critical current density, and the characteristic resistance of MS $R_N A$, $\lambda_J = (\hbar/2e\mu_0 d j_C)^{1/2}$ is Josephson penetration depth at $T = 4.2$ K, $H = 0$.

L (μm)	d (nm)	I_C (μA)	R_N (Ω)	$R_N A$ (Ωcm^2)	j_C (A/cm^2)	$I_C R_N$ (μV)	λ_J (μm)
50	7	6.5	5.0	125	0.26	32	725
40	7	6.0	7.1	114	0.38	43	600
30	7	3.0	10.4	94	0.33	31	645
20	7	0.5	20.7	83	0.12	10	1065
50	5	35	0.5	12.5	1.4	17.5	305
40	5	70	0.7	11.2	4.4	49	172

while the amount of j_C increases, keeping the $I_C R_N$ product unchanged (see Table I).

The I - V curves were transformed as shown in Fig. 3(c) when magnetic field was applied. Magnetic-field dependence of superconducting critical current $I_C(H)$ showed a sharp central peak and minor oscillating behavior for sidelobes [see Fig. 3(d)]; the theoretical Fraunhofer dependence $I_C(H) = I_0 |\sin(\pi H)/\pi H|$ [35] is also given in Fig. 3(c). The calculated magnetic-field level which corresponds to the first minimum of the Fraunhofer pattern is $H_1 = \Phi_0/\mu_0 d_j L \simeq 4$ Oe, where $d_j = d + \lambda_{\text{Nb}} c \tanh(d_{\text{Nb}}/2\lambda_{\text{Nb}}) + \lambda_{\text{YBCO}} c \tanh(d_{\text{YBCO}}/2\lambda_{\text{YBCO}})$, $d = 7$ nm is thickness of Sr_2IrO_4 barrier, $L = 50 \mu\text{m}$ is junction size, and $\lambda_{\text{YBCO}} = 150$ nm, $\lambda_{\text{Nb}} = 90$ nm are London penetration depths for YBCO and Nb at 4.2 K, correspondingly. From Fig. 3(d) it is seen that the

experimental H_1 is smaller than the predicted one, and the half-width at the half-height of the central peak is narrower than that calculated for the case of a tunnel junction [36] with the geometry and magnetic-field direction as in our experiment. The observed dependence $I_C(H)$ with well-defined zeros indicates the absence of pinholes in MS. Although Sr_2IrO_4 has weak magnetic moment a minor shift of maximum $I_C(H)$ does not exceed uncertainty of applied magnetic field, which could be caused by the influence of weak residual magnetic field of multium mu-metal foil. An enhanced sensitivity of the superconducting current to magnetic field has been observed earlier for the junctions with the antiferromagnetic $\text{Ca}_{0.5}\text{Sr}_{0.5}\text{CuO}_2$ interlayer [37,38].

In MS the s -wave Nb/Au superconducting electrode contacts via the Sr_2IrO_4 interlayer with the YBCO superconductor whose order parameter is described as a

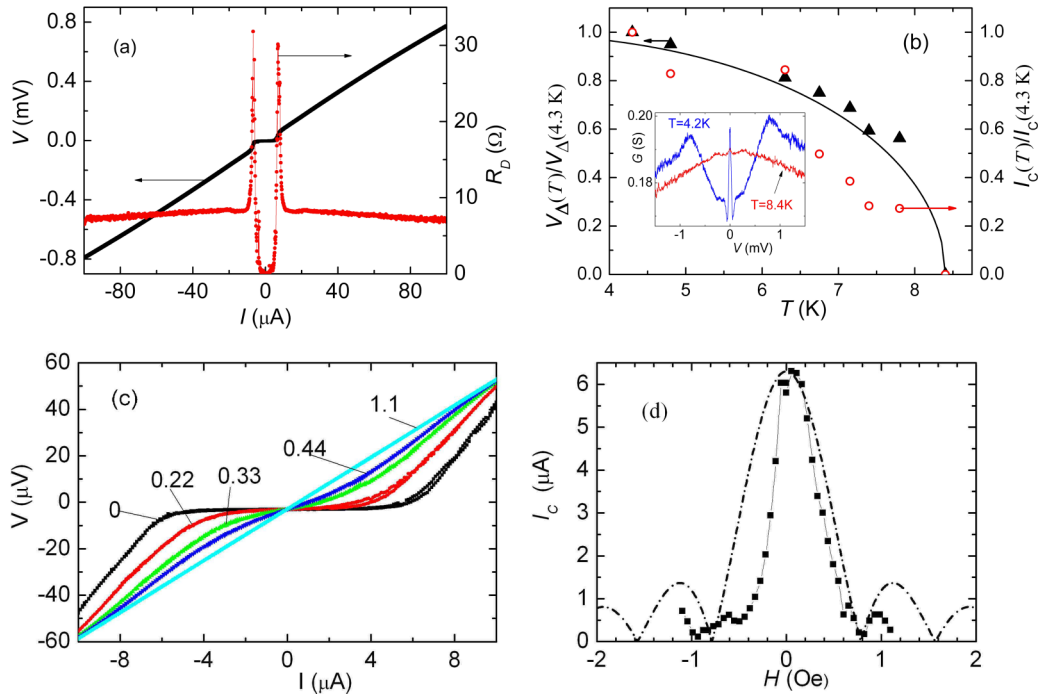


FIG. 3. (a) I - V curve and differential resistance $R_D = dV/dI$ versus current I . The critical current is determined by the local maxima of dV/dI . (b) Temperature dependences of the normalized critical current I_C and gap voltage V_Δ . A solid line is the BCS dependence of the energy gap versus temperature. Inset shows singularities on dV/dI (V) caused by the energy gap of the Nb electrode at $T = 4.2$ and 8.4 K. (c) Family of I - V curves at $T = 4.2$ K and magnetic field varied in the range 0–1.1 Oe for MS with $L = 50 \mu\text{m}$ and $d = 7$ nm. (d) Critical current versus the magnetic field (black squares). The calculated Fraunhofer pattern (shown by dashed-dotted line) $I_C(H) = I_0 |\sin(\pi H)/\pi H|$, where $H = \Phi/\mu_0 d_j$ for the sandwich-type junction with $L = 50 \mu\text{m}$ and $d = 7$ nm.

superposition of d -wave (Δ_d) and s -wave (Δ_s) components: $\Delta(\theta) = \Delta_d \cos 2\theta + \Delta_s$, where θ is the angle between the quasiparticle momentum and the a axis of the YBCO [39–41]. In the case of Nb/Au/YBCO junction the superconducting current-phase relation may differ from the sinusoidal one, particularly for the transport along the c direction D_{001} [39–41]:

$$I_s(\varphi) = I_{c1} \sin \varphi + I_{c2} \sin 2\varphi, \quad (1)$$

where I_{c1} and I_{c2} are amplitudes of the critical current for the first and the second harmonics, and the ratio $q = I_{c2}/I_{c1}$ is used as a characteristic parameter for the second harmonic in the CPR. The d -wave component of the YBCO superconducting order parameter (Δ_d) promotes the unconventional superconducting CPR of the junction with the second-harmonic amplitude [31]. We can see from Ref. [31] that at small $q \leq 0.5$ the difference between I_{c1} and I_C is less than 20% but it increases for $q > 0.5$ [42]. The first harmonic I_{c1} originates from the minor s -wave component of the superconducting order parameter in YBCO (Δ_s) and in the case $\Delta_d \gg \Delta_s$, Δ_{Nb} it looks like [39]

$$I_{c1} R_N \approx \Delta_s \Delta_{\text{Nb}} / (e \Delta_D^*), \quad (2)$$

where e is electron charge, $\Delta_D^* = \pi \Delta_d [2 \ln(3.56 \Delta_d / k_B T_{c\text{Nb}})]^{-1}$, and k_B is Boltzmann constant. For MS with $V_\Delta (4.2 \text{ K}) \approx 0.8 \text{ mV}$ the parameters $\Delta_{\text{Nb}}/e \approx \Delta_s/e$ are also 0.8 mV and taking typical value $\Delta_d/e \approx 20 \text{ mV}$ for YBCO we get $I_{c1} R_N \approx 60 \mu\text{V}$ calculated by Eq. (2). It is twice larger than the experimentally obtained values of $I_C R_N$ (see Table I), and close to S/D_{001} junctions without interlayer [31]. Thus, inserting the Sr_2IrO_4 interlayer between YBCO and Au/Nb results just in reduction of the $I_{c1} R_N$ product.

Note, superconducting current was absent in mesas with the interlayer made of any of ferromagnetic manganites $\text{La}_{0.7}\text{Sr}_{0.3}\text{MnO}_3$, $\text{La}_{0.7}\text{Ca}_{0.3}\text{MnO}_3$, or LaMnO_3 ($3d$ material) even at reduced temperatures below $T < 4.2 \text{ K}$ [43]. Thus, specific properties of Sr_2IrO_4 , which is $5d$ material with strong SOI, should be taken into account [44].

Oxygen migration at $\text{Sr}_2\text{IrO}_4/\text{YBCO}$ interface could play the decisive role for appearance of superconducting current in MS through the thick Sr_2IrO_4 interlayer (in comparison with the coherence length). According to experimental data [44] even a minor change in the oxygen content in Sr_2IrO_4 leads to a drastic change in the conductivity type of Sr_2IrO_4 at low temperature from activation to metallic. Figure 4 shows evolution of conductivity $G(V)$ with temperature, demonstrating zero-bias conductance peak (ZBCP) up to $T = 48 \text{ K}$ for MS with $d = 7 \text{ nm}$, $L = 40 \mu\text{m}$. Existence of ZBCP in experimental data shows that the $\text{Sr}_2\text{IrO}_4/\text{YBCO}$ interface is quite transparent and low-energy states occurred, and the interface $\text{Sr}_2\text{IrO}_4/\text{YBCO}$ could be considered as N_{SO}/S , where N_{SO} is a normal metal with SOI, S is a singlet superconductor. Taking into account the rise of conductance $G(V)$ at $V > 10 \text{ mV}$ and low temperatures (see Fig. 4) which is inherent to an existence of barrier I between Sr_2IrO_4 and Au/Nb superconducting (S') bilayer, the whole MS could be modeled as $S'/I/N_{\text{SO}}/S$. Appearance of Andreev states at interface of spin-singlet superconductor and a conductor with Rashba-type spin-orbit interaction may lead to removed spin degeneracy without the help of magnetic field [45], and predicted effects [1–9] for a

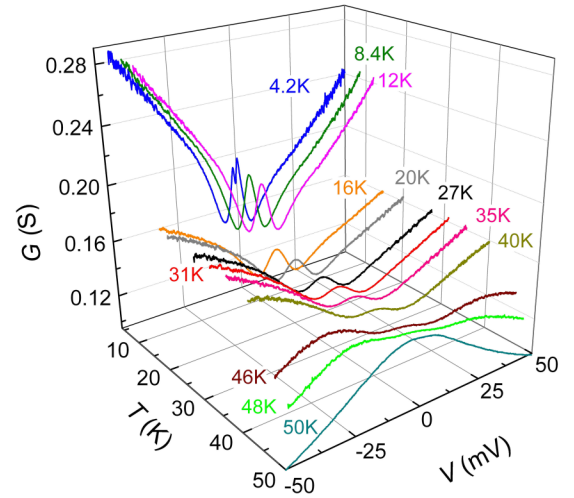


FIG. 4. Voltage dependence of conductivity $G(V)$ for mesa-structure with $d = 7 \text{ nm}$, $L = 40 \mu\text{m}$ at temperatures $T = 4.2 - 50 \text{ K}$.

junction of spin-singlet superconductor YBCO and Sr_2IrO_4 with strong SOI [28] could be relevant. When SOI is taken into account at the $\text{Sr}_2\text{IrO}_4/\text{YBCO}$ interface [46] a spin-triplet component of superconducting current may occur along with the long range proximity effect. Particularly, theoretical models [8,9] for singlet-triplet conversion could be considered. Recently in Ref. [47] was shown that with an increase of SOI the decay length of superconducting correlations can be significantly increased even in the absence of exchange field. In accordance to Ref. [9] in the case of large energy of spin-orbit interaction, comparable with Fermi energy $E_{\text{SO}} \sim E_F$, the decay length of pairing amplitudes ξ for the case of spin-triplet component becomes of order l_{SO} , the spin-orbit length. At the same time, theory [9] predicts enhancement for both spin-singlet and spin-triplet components with increase of SOI strength, and if $E_{\text{SO}} = 0$ the triplet component is absent, but the singlet exists. Comparing critical current densities j_C for d with 5 and 7 nm, and assuming an exponential decay for characteristic length of superconducting current in MS, it becomes of order of $\xi \sim 1 \text{ nm}$. However, a question of which components, singlet, triplet, or both survive over 7-nm-thick Sr_2IrO_4 in $S'/I/N_{\text{SO}}/S$ -type mesas remains unanswered yet.

One should note that in a superconducting junction with antiferromagnetic barrier, modeled by thin (much smaller than the coherence length) separated from each other ferromagnetic layers with opposite magnetization and placed in perpendicular relative to superconducting electrodes, the long-range superconducting proximity effect with spin-singlet pairing also takes place [37,48,49]. However, the model [49] hardly could explain our experimental data as it differs by geometry of antiferromagnetic barrier in which the exchange interaction of ferromagnetic layers should be of few meV—considerably smaller than the energy of SOI in $\text{Sr}_2\text{IrO}_4 \sim 0.4 \text{ eV}$.

B. Microwave measurements

The information on CPR in MS could be obtained from the dynamics of Shapiro steps by varying the power of microwave irradiation at high-frequency limit $f_e > f_C$ [31,50].

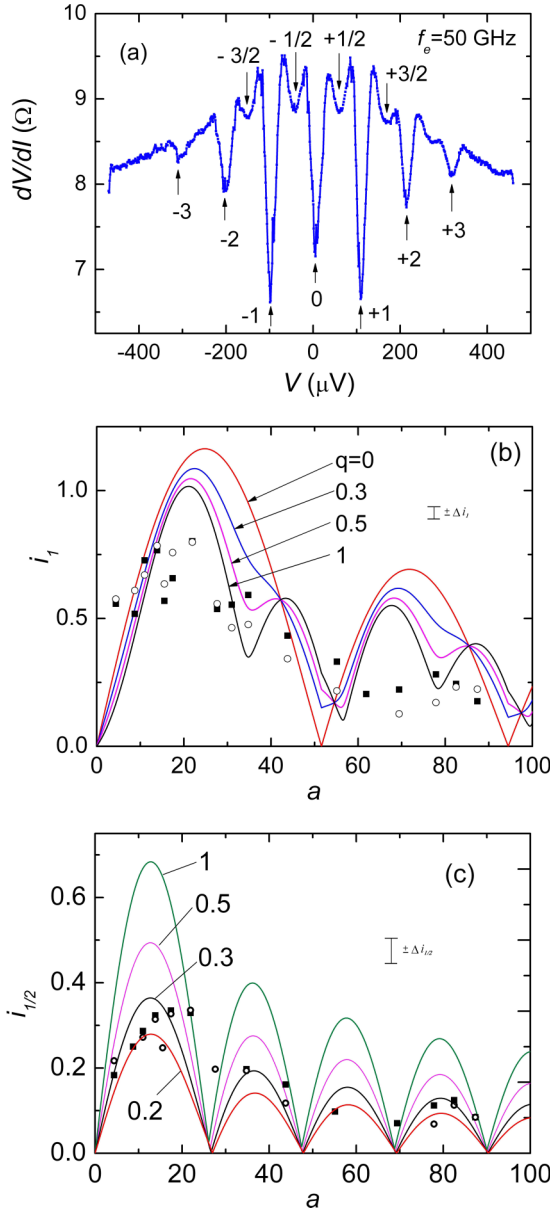


FIG. 5. (a) Voltage dependence of the differential resistance $R_D = dV/dI$ for the MS with $d = 7$ nm, $L = 40$ μm , $T = 4.2$ K under influence of microwave radiation with frequency $f_e = 50$ GHz. The arrows and numbers indicate the position of integer ($n = m = 1$) and fractional Shapiro steps ($n = 1, m = 2$) at voltages $V_{n,m} = (n/m)hf_e/2e$. The number “0” corresponds to the critical current. (b) Normalized amplitudes of the first $i_1 = I_1(a)/I_C(0)$ Shapiro step. Theoretical curves were calculated taking $a = I_{MW}/I_C$ as a fitting parameter for ratios $q = I_{c2}/I_{c1} = 0, 0.3, 0.5, 1$ and McCumber parameter $\beta_C = 1$. Error bar is indicated by $\pm \Delta i_1$. (c) Normalized amplitudes of half-integer Shapiro steps $i_{1/2} = I_{1/2}(a)/I_C(0)$. Error bar is indicated by $\pm \Delta i_{1/2}$. Theoretical curves were calculated for $q = 0.2, 0.3, 0.5, 1$, and $\beta_C = 1$. Open and closed symbols correspond to positive and negative voltage biasing.

Since the characteristic frequency for MS $f_C = (I_C R_N)2e/h$ (h is Planck’s constant) is in GHz range the measurements were carried out at high enough frequencies at $f_e = 38$ GHz, or $f_e = 50$ GHz. The voltage dependence of dV/dI of MS

at $f_e = 50$ GHz demonstrated both integer and fractional Shapiro steps arising due to synchronization between Josephson oscillations and the external microwaves at voltages $V_{n,m} = (n/m)hf_e/2e$ [see Fig. 5(a)]. The fractional Shapiro steps may indicate the presence of the second harmonic in CPR $I_{c2} \neq 0$. Figures 5(b) and 5(c) show dependences of the first $i_1 = I_1/I_C$ ($n = m = 1$), and the fractional (half integer) $i_{1/2} = I_{1/2}/I_C$ ($n = 1, m = 2$) Shapiro steps from normalized microwave current $a = I_{MW}/I_C(0)$ at $f_e = 50$ GHz, correspondingly. The dependences of $i_1(a)$ and $i_{1/2}(a)$ calculated for different values of $q = I_{c2}/I_{c1}$ using the modified resistively shunted junction model [31,50] are also shown. Experimental data demonstrated well-defined local max for $i_1(a)$ at $a \approx 20$ and a minor one at $a \approx 80$. Note, for $q > 0$ the minima of theoretical function $i_1(a)$ do not reach $i_1 = 0$, but the $i_{1/2}(a)$ does. Deviation of experimental $i_1(a)$ dependence from theoretical could be attributed to the presence of higher harmonics in CPR, as well by the impact of enhanced strong nonstationary processes which are not considered in the model [31,50]. Taking the maximal amplitude of experimental dependence $i_{1/2}(a) \approx 0.3$, the best fit for half-integer Shapiro step corresponds to the theoretical function for $q = 0.3$.

The d -wave component of the YBCO superconducting order parameter (Δ_d) promotes the unconventional superconducting CPR of the junction with the second-harmonic amplitude [31]

$$I_{c2}R_N \approx \Im \Delta_{Nb}/e. \quad (3)$$

The contribution of the second harmonic caused by the d -wave symmetry for S/D_{001} junction with the same electrical parameters as the discussed MS with $L = 40$ μm gives $I_{c2} \approx 20$ nA for $\Im = 2 \times 10^{-4}$, $\Delta_{Nb}/e = 0.8$ mV, and $R_N = 7.1$ Ω at $T = 4.2$ K. Using the theoretical dependence for ratio I_{c1}/I_C versus q [31,42] and the estimated “ d -wave” contribution of I_{c2} , it gives negligibly small $q \approx 3 \times 10^{-3}$.

The deviation of CPR from sinusoidal may originate due to appearance at the $\text{Sr}_2\text{IrO}_4/\text{YBCO}$ interface of the low-energy states, related to the coherent Andreev reflections [9,27,28,51,52]. Indeed, the MS demonstrated the zero-bias conductivity peak at temperatures $T = 4.2$ K as well at temperatures $T > T_{CNb}$ which could be associated with low-energy states. At the same time a tunneling-type conductivity is seen at higher voltages $V > 10$ mV at low temperatures along with asymmetry of $G(V)$ dependence. Note, the theoretical simulation [28] shows that the interface of cuprate superconductor with the Sr_2IrO_4 could exhibit both helical Majorana fermions and zero-energy flat edge states. However, the origin of the ZBCP and the asymmetry of $G(V)$ in the MS require additional studies.

IV. SUMMARY

In conclusion, Nb/Au/ $\text{Sr}_2\text{IrO}_4/\text{YBa}_2\text{Cu}_3\text{O}_x$ mesostructures with epitaxial bilayer of Sr_2IrO_4 and $\text{YBa}_2\text{Cu}_3\text{O}_x$ films have been fabricated. The superconducting current for the thickness 5 and 7 nm of Sr_2IrO_4 interlayer has been observed. The critical current of the meso-structure increased with decreasing temperature similarly as the voltage of the gap singularity of Nb film. Under weak magnetic field

the $I_C(H)$ dependence showed a sharp central peak and minor oscillating behavior for sidelobes as in the case of the absence of pinholes in the interlayer. Under the influence of electromagnetic radiation at millimeter-frequency band, the Shapiro steps at both multiple and fractional quantities $(n/m)hf_e/2e$ of voltages were observed, indicating the deviation of the current-phase relation from the sinusoidal and the presence of the second harmonic, which could not be explained solely by impact of d -wave symmetry of c -oriented YBCO electrode.

ACKNOWLEDGMENTS

The authors gratefully acknowledge I. V. Borisenko, L. V. Filippenko, and D. Winkler for the help and useful discussions. The work was carried out within the framework of the Russian state task and partially supported by the Russian Foundation for Basic Research, projects 19-07-00274, and 19-07-00143. G.A.O. and A.V.S. would like to acknowledge COST Action MP1308 - TO-BE for Short-Term Scientific Mission (STSM) program.

-
- [1] M. Eschrig, *Rep. Prog. Phys.* **78**, 104501 (2015).
- [2] J. Linder and J. W. A. Robinson, *Nat. Phys.* **11**, 307 (2015).
- [3] M. Horsdal, G. Khaliullin, T. Hyart, and B. Rosenow, *Phys. Rev. B* **93**, 220502(R) (2016).
- [4] F. S. Bergeret and I. V. Tokatly, *Phys. Rev. B* **89**, 134517 (2014).
- [5] S. H. Jacobsen and J. Linder, *Phys. Rev. B* **92**, 024501 (2015).
- [6] F. Konschelle, I. V. Tokatly, and F. S. Bergeret, *Eur. Phys. J. B* **87**, 119 (2014).
- [7] F. S. Bergeret, A. F. Volkov, and K. B. Efetov, *Rev. Mod. Phys.* **77**, 1321 (2005).
- [8] I. V. Bobkova and A. M. Bobkov, *Phys. Rev. B* **95**, 184518 (2017).
- [9] C. R. Reeg and D. L. Maslov, *Phys. Rev. B* **92**, 134512 (2015).
- [10] R. Yano, M. Koyanagi, H. Kashiwaya, K. Tsumura, H. Hirose, Y. Asano, T. Sasagawa, and S. Kashiwaya, [arXiv:1805.10435v1](https://arxiv.org/abs/1805.10435v1).
- [11] J. D. Sau, R. M. Lutchyn, S. Tewari, and S. Das Sarma, *Phys. Rev. Lett.* **104**, 040502 (2010).
- [12] H. J. Suominen, J. Danon, M. Kjaergaard, K. Flensberg, J. Shaban, C. J. Palmstrøm, F. Nichele, and C. M. Marcus, *Phys. Rev. B* **95**, 035307 (2017).
- [13] D. Sun and J. Liu, *Phys. Rev. B* **97**, 035311 (2018).
- [14] F. Domínguez, O. Kashuba, E. Bocquillon, J. Wiedenmann, R. S. Deacon, T. M. Klapwijk, G. Platero, L. W. Molenkamp, B. Trauzettel, and E. M. Hankiewicz, *Phys. Rev. B* **95**, 195430 (2017).
- [15] J. Wiedenmann, E. Bocquillon, R. S. Deacon, S. Hartinger, O. Herrmann, T. M. Klapwijk, L. Maier, C. Ames, C. Brune, C. Gould, A. Oiwa, K. Ishibashi, S. Tarucha, H. Buhmann, and L. W. Molenkamp, *Nat. Commun.* **7**, 10303 (2016).
- [16] C. J. Pedder, T. Meng, R. P. Tiwari, and T. L. Schmidt, *Phys. Rev. B* **96**, 165429 (2017).
- [17] S. J. Moon, H. Jin, K. W. Kim, W. S. Choi, Y. S. Lee, J. Yu, G. Cao, A. Sumi, H. Funakubo, C. Bernhard, and T. W. Noh, *Phys. Rev. Lett.* **101**, 226402 (2008).
- [18] W. Witzak-Krempa, G. Chen, Y. B. Kim, and L. Balents, *Annu. Rev. Condens. Matter Phys.* **5**, 57 (2014).
- [19] R. Schaffer, E. Lee, B. Yang, and Y. Kim, *Rep. Prog. Phys.* **79**, 094504 (2016).
- [20] E. E. Gordon, H. Xiang, J. Köhler, and M.-H. Whangbo, *J. Chem. Phys.* **144**, 114706 (2016).
- [21] Y. Gim, A. Sethi, Q. Zhao, J. F. Mitchell, G. Cao, and S. L. Cooper, *Phys. Rev. B* **93**, 024405 (2016).
- [22] Y. K. Kim, N. H. Sung, J. D. Denlinger, and B. J. Kim, *Nat. Phys.* **12**, 37 (2016).
- [23] S.-i. Hikino, *J. Phys. Soc. Japan*, **87**, 074707 (2018).
- [24] G. A. Ovsyannikov, A. S. Grishin, K. Y. Constantinian, A. V. Shadrin, A. M. Petrzhik, Yu. V. Kislinkii, G. Cristiani, and G. Logvenov, *Phys. Solid State* **60**, 2166 (2018).
- [25] A. M. Petrzhik, G. Cristiani, G. Logvenov, A. E. Pestun, N. V. Andreev, Yu. V. Kislinkii, and G. A. Ovsyannikov, *Tech. Phys. Lett.* **43**, 554 (2017).
- [26] H. Wang, S.-L. Yu, and J.-X. Li, *Phys. Rev. B* **91**, 165138 (2015).
- [27] S. Takei, B. M. Fregoso, V. Galitski, and S. Das Sarma, *Phys. Rev. B* **87**, 014504 (2013).
- [28] Y. Chen, and H.-Y. Kee, *Phys. Rev. B* **97**, 085155 (2018).
- [29] N. Satchell and N. O. Birge, *Phys. Rev. B* **97**, 214509 (2018).
- [30] C. Lu, A. Quindeau, H. Deniz, D. Preziosi, D. Hesse, and M. Alexe, *Appl. Phys. Lett.* **105**, 082407 (2014).
- [31] P. Komissinskiy, G. A. Ovsyannikov, K. Y. Constantinian, Y. V. Kislinkii, I. V. Borisenko, I. I. Soloviev, V. K. Kornev, E. Goldobin, and D. Winkler, *Phys. Rev. B* **78**, 024501 (2008).
- [32] See Supplemental Material at <http://link.aps.org/supplemental/10.1103/PhysRevB.100.024501> for x-ray measurements, resistivity of Sr₂IrO₄ films, and approach used for determination of small amplitudes of critical current and Shapiro steps.
- [33] K. K. Likharev, *Dynamics of Josephson Junctions and Circuits* (OPA Ltd. for Gordon and Breach Publishers, New York, 1986).
- [34] H. Kanter and F. L. Vernon, *Phys. Rev. B* **2**, 4694 (1970).
- [35] A. Barone and G. Paternò, *Physics and Applications of the Josephson Effect* (Wiley, New York, 1982), p. 529.
- [36] R. Monaco, M. Aaroe, J. Mygind, and V. P. Koshelets, *J. Appl. Phys.* **104**, 023906 (2008).
- [37] Yu. V. Kislinkii, P. V. Komissinskiy, K. Y. Constantinian, G. A. Ovsyannikov, T. Yu. Karminskaya, I. I. Soloviev, and V. K. Kornev, *J. Exp. Theor. Phys.* **101**, 494 (2005).
- [38] A. V. Zaitsev, G. A. Ovsyannikov, K. Y. Constantinian, Yu. V. Kislinkii, A. V. Shadrin, I. V. Borisenko, and P. V. Komissinskiy, *J. Exp. Theor. Phys.* **110**, 336 (2010).
- [39] P. V. Komissinskiy, E. Il'ichev, G. A. Ovsyannikov, S. A. Kovtonyuk, M. Grajcar, R. Hlubina, Z. Ivanov, Y. Tanaka, N. Yoshida, and S. Kashiwaya, *Europhys. Lett.* **57**, 585 (2002).
- [40] A. Blais and A. M. Zagorskin, *Phys. Rev. A* **61**, 042308 (2000).
- [41] Y. Tanaka and S. Kashiwaya, *Phys. Rev. B* **53**, R11957 (1996).
- [42] E. Goldobin, D. Koelle, R. Kleiner, and A. Buzdin, *Phys. Rev. B* **76**, 224523 (2007).

- [43] A. M. Petrzlik, G. A. Ovsyannikov, A. V. Shadrin, K. Y. Konstantinyan, A. V. Zaitsev, V. V. Demidov, and Yu. V. Kislinskii, *J. Exp. Theor. Phys.* **112**, 1042 (2011).
- [44] O. B. Korneta, T. Qi, S. Chikara, S. Parkin, L. E. De Long, P. Schlottmann, and G. Cao, *Phys. Rev. B* **82**, 115117 (2010).
- [45] A. A. Reynoso, G. Usaj, C. A. Balseiro, D. Feinberg, and M. Avignon, *Phys. Rev. B* **86**, 214519 (2012).
- [46] M. Horsdal and T. Hyart, *Sci. Post Phys.* **3**, 041 (2017).
- [47] Y. Lu and T. T. Heikkilä, [arXiv:1905.11135](https://arxiv.org/abs/1905.11135).
- [48] P. Komissinskiy, G. A. Ovsyannikov, I. V. Borisenko, Yu. V. Kislinskii, K. Y. Constantinian, A.V. Zaitsev, and D. Winkler, *Phys. Rev. Lett.* **99**, 017004 (2007).
- [49] L. Gorkov and V. Kresin, *Appl. Phys. Lett.* **78**, 3657 (2001).
- [50] V. K. Kornev, T. Y. Karminskaya, Y. V. Kislinski, P. V. Komissinki, K. Y. Constantinian, and G. A. Ovsyannikov, *Physica C* **435**, 27 (2006).
- [51] C.-K. Chiu and S. Das Sarma, *Phys. Rev. B* **99**, 035312 (2019).
- [52] A. Haim and Y. Oreg, [arXiv:1809.06863v1](https://arxiv.org/abs/1809.06863v1).